

Article

Mustard Gold of the Gaching Ore Deposit (Maletoyvayam Ore Field, Kamchatka, Russia)

Nadezhda D. Tolstykh ^{1,2,*}, Galina A. Palyanova ^{1,2} , Ol'ga V. Bobrova ³ and Evgeny G. Sidorov ⁴

¹ VS Sobolev Institute of Geology and Mineralogy of Siberian Branch of Russian Academy of Sciences, Koptiyuga Ave., 3, 630090 Novosibirsk, Russia

² Department of Geology and Geophysics, Novosibirsk State University, Pirogova Ave., 2, 630090 Novosibirsk, Russia

³ Coralina Engineering, Poslannikov per., 5, 105005 Moscow, Russia

⁴ Institute of Volcanology and Seismology, Far East Branch of Russian Academy of Sciences, Piipa Blvd., 9, 683006 Petropavlovsk-Kamchatsky, Russia

* Correspondence: tolst@igm.nsc.ru

Received: 1 July 2019; Accepted: 8 August 2019; Published: 15 August 2019



Abstract: The Gaching high-sulfidation (HS) epithermal Au–Ag deposits, part of the Maletoyvayam ore field, which is located in the volcanic belts of the Kamchatka Peninsula (Russia). The main ore components are native gold, tellurides, selenides, and sulphoselenotellurides of Au and oxidation products of Au-tellurides. This study examines the different types of native gold in this ore deposit and the mechanisms and sequential transformation of calaverite (AuTe₂) into mustard gold. The primary high fineness gold (964‰–978‰) intergrown with maletoyvayamite Au₃Te₆Se₄ and other unnamed phases (AuSe, Au(Te,Se)) differ from the secondary (mustard) gold in terms of fineness (1000‰) and texture. Primary gold is homogeneous, whereas mustard is spongy. Two types of mustard gold were identified: (a) Mixtures of Fe-Sb(Te,Se,S) oxides and fine gold particles, which formed during the hypogenic transformation stage of calaverite due to the impact of hydrothermal fluids, and (b) spotted and colloform gold consisting of aggregates of gold particles in a goethite/hydrogoethite matrix. This formed during the hypergenic transformation stage. Selenides and sulphoselenotellurides of gold did not undergo oxidation. Pseudomorphic replacement of calaverite by Au-Sb(Te,Se,S,As) oxides was also observed.

Keywords: Gaching ore deposit; mustard gold; calaverite; maletoyvayamite; Fe-Sb(Te,As,Se,S)-oxides; Au-Sb(Te,Se,S,As)-oxides

1. Introduction

One of the fundamental tasks in the study of the epithermal deposits is identifying the mechanisms of gold formation. The traditional gravity method can sometimes give negative results in the identifying of the cause of the high Au concentrations. Occasionally sample analyses show high concentrations of Au, while the presence of visible gold is absent or is only represented by single grains where the amount of Au is not capable the providing such high concentrations. It appears that the finest fraction (<0.06 mm) is the most enriched in Au, which is almost beyond visible detection. The high concentrations of Au in the hypergenesis zones of epithermal deposits is due to the presence of so-called mustard gold, which is difficult to detect.

The term “mustard gold” was introduced by W. Lindgren [1]. Typical features of mustard gold are low reflectivity, porous or colloform texture, and rusty, reddish, orange-red, and brown-yellow colors in reflected light. Mustard gold is easily scattered during crushing and the resulting fine powdered fraction may become progressively enriched in gold. Mustard gold was previously studied by numerous

researchers [2–8] and has been shown to be a characteristic feature in gold-telluride deposits [9,10] and antimony-gold deposits [11,12]. Mustard gold was also documented in the Ozernovskoye and Aginskoye deposits (Kamchatka) as rims surrounding primary Au tellurides or as micro-veinlets in the altered matrix [4,6]. These deposits belong to the alunite-quartz group of the gold-silver deposits (Figure 1) and are associated with metasomatic rocks (secondary quartzites) that are confined to the volcanic centers of volcanic-tectonic structures within the Vetrovayam volcanic zone. Mustard gold is formed due to the oxidation of primary Au minerals and is the result of exposure to acidic solutions leaching tellurium or their transformation into tellurates [2,3]. This replacement may take place under hydrothermal conditions, such as during the late-stages of ore deposit formation [5]. The development of microporous gold indicates that the deposits may have experienced overprint after mineralization [13]. Mustard gold is heterogeneous and represented by multiphase aggregates consisting of two, three, or more phases, which differ in their chemical composition. Typomorphic elements in these compounds within the pores of mustard gold include Sb, Te, Pb, Fe, Cu, Ag, Hg, and others, which are dependent on the composition of the primary mineral assemblage of the deposit. Mustard gold intergrowths with Au-sulfoselenotellurides, sulfosalts (tetrahedrite, goldfieldite), and the products of oxidation of Au-tellurides from the Gaching deposit of the Maletovvayam ore field in the volcanic belts of the Kamchatka Peninsula (Figure 1) are presented in this study [14].

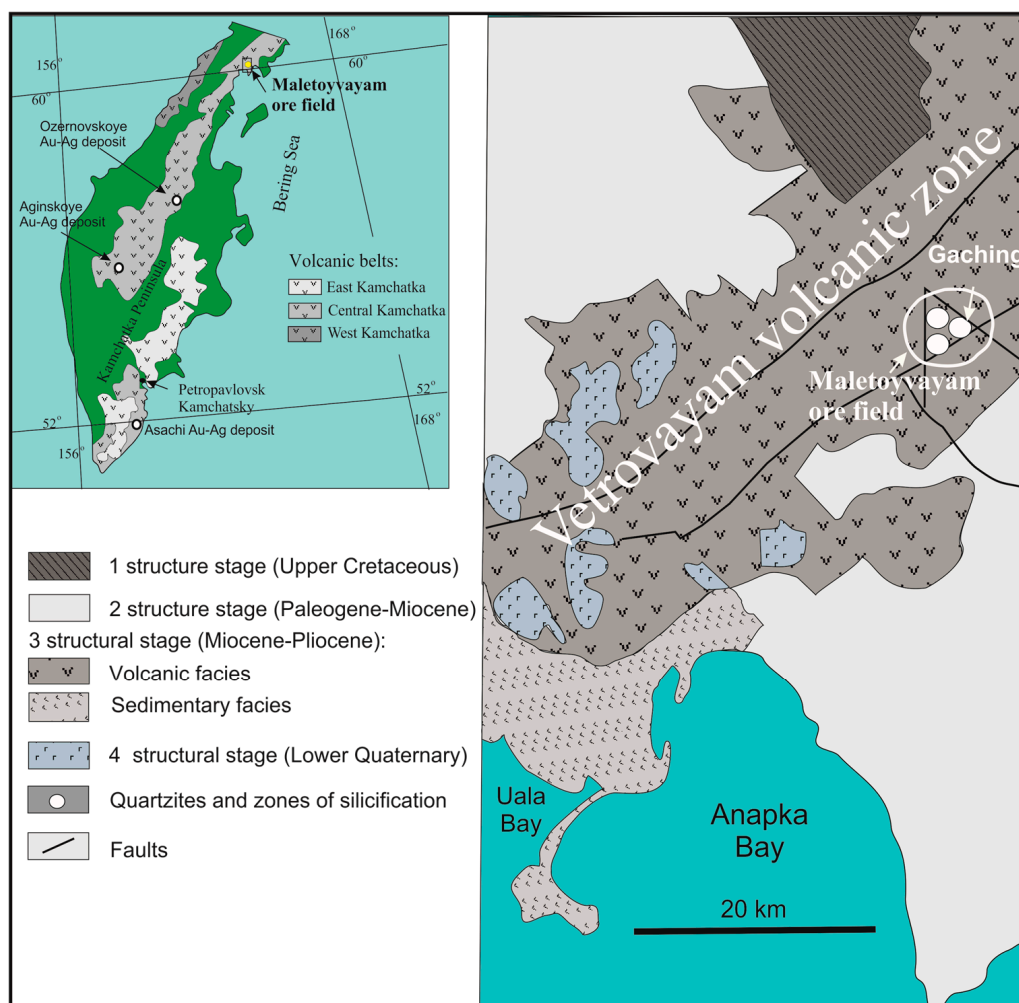


Figure 1. Volcanic belts of the Kamchatka Peninsula [15], the tectonic scheme of the Vetrovayam volcanic zone [16] and location of Maletovvayam ore field on the base [17] (reproduced with permission from reference [14]).

This study presents detailed textural descriptions, chemical compositions and reconstructs the sequence of replacement of primary minerals in order to understand its origin. Our research shows a sequential transformation of the primary mineralization, which is represented by calaverite to mustard gold.

2. Materials and Methods

The studied grains of Au-minerals were obtained by crushing mineralized rocks and panning the resulting material into a heavy fraction using hydroseparation, followed by concentration in the heavy liquid. Mustard gold was found in polished sections made from the heavy mineral concentrate, which was obtained from a 20-kilogram sample of alunite-quartz rock. The chemical compositions of the minerals, mineral aggregate textures, and separated grains were examined at the Analytical Center for Multi-Elemental and Isotope Research at the VS Sobolev Institute of Geology and Mineralogy SB RAS in Novosibirsk (Russia) using a LEO-413VP scanning electron microscope (SEM) with INCA Energy 350 microanalysis system (Oxford Instruments Ltd., Abingdon, UK) equipped with EDS (analysts Dr. N. Karmanov, M. Khlestov, and V. Danilovskaya), operating at an accelerating voltage of 20 kV, beam current of 0.4 nA, 50 s measuring time, and beam diameter of ~1 μm . The following standards were used: Pure substances (Ag, Au, Bi, Se, Sb, Fe, and Cu), pyrite (S), synthetic HgTe (Te), and sperrylite (As). The detection limit was 0.02%. The following X-ray lines were selected: $L\alpha$ for Ag, Te, As, Sb, and Se; $K\alpha$ for S, Fe, Cu, and O; and $M\alpha$ for Au and Bi. All the compositions of minerals in this study were performed using an EDS spectrometer. A compositional comparison Au–Te–Se–S minerals determined by the EDS and WDS methods is presented in a previous study [14], which shows their complete convergence.

3. Results

3.1. Types of Mustard Gold

Previous studies of the Gaching ore deposit that refer to the epithermal Au–Ag high-sulfidation (HS) type have identified native gold, barite, anglesite, quartz, pyrite, Au-telluride (Se-bearing calaverite), Au-sulphoselenotellurides, sulphosalts (tetrahedrite, goldfieldite, tennantite), and other rare minerals (famatinite, enargite, watanabeite, senarmontite, tripuhyite, rooseveltite, tiemanite, antimonsilite, and guanajuatite) in heavy fractions [14]. Over 200 grains of Au–Te–Se–S compounds were additionally extracted from the ore to obtain new data.

The studied grains of primary Au–Ag alloys (10–50 μm in size) are always found as intergrowths with sulfosalts or unique unnamed phases of the Au–Te–Se–S system that are potentially new minerals with unique compositions: $\text{Au}_3\text{Te}_6(\text{Se,S})_4$, $\text{Au}_2\text{Te}_4(\text{Se,S})_3$, AuSe, Au_2TeSe , and other (Figure 2a,b) [14,18]. One of these minerals, $\text{Au}_3\text{Te}_6\text{Se}_4$, was recently approved by a commission on new minerals and named maletoyvayamite [19]. The possibility of natural occurrences of compounds of Te, Se, and S and Ag was previously shown in the Prasolovskoye deposit on Kunashir Island [3,20].

Primary gold in the Gaching deposit occurs in high grades and Ag does not exceed 2.5 wt. % [14]. In the studied samples (Figure 2), Ag-content varied in range 1.47–1.98 wt. % (Tables 1 and 2). Neither primary gold, nor these compounds undergo replacement or oxidation during hypogene processes. It should be noted that direct intergrowths of primary gold with calaverite (AuTe_2) or mustard gold was not found. Primary gold (Au–Ag alloys) in the Gaching deposit accounts for no more than 5% when the porous gold reaches up to 60% of the amount of the Au-bearing minerals in the ore assemblage. Mustard gold exhibited more yellowish, reddish, and brown colors in reflected light (Figure 3) when compared to primary gold (Figure 3c) and porous texture gold, as observed in the other deposits worldwide. Irregular grains of mustard gold are between 10 and 60 μm in size and exhibited spongy textures, which were either empty or imbedded with microscopic inclusions in the pore spacings (Figure 4), similar to mustard gold from the Dongping Au–Te deposit [9,10,13]. Mustard gold varied from microporous (i.e., spongy) to colloform and zoned. However, microporous aggregates of gold

filled by compounds of Fe, Sb, Te, As, Bi, and S with oxygen (antimonate/tellurate of iron; Figure 4) were prevalent. The contents of these compounds in microporous gold were due to the weathering of minerals (mainly sulfosalts). The presence of Ag in these compounds was likely due to inheritance from primary calaverite. At this stage of mustard gold formation, Ag is a minor element that enters oxides, since analyses of larger fragments of secondary mustard gold showed the complete absence of Ag in its composition (Table 3), sample d_9-6). Analyses of these compounds mixed with gold particles are presented in Table 3. The types of mustard gold were identified by contents of various antimonate/tellurate/hydroxides in the submicroscopic pores of the mustard gold aggregate. As shown in Table 1, all elements showed great compositional variation. The oxygen concentration also changed due to (1) different degrees of oxidation of the primary products, and (2) different ratios of secondary gold and Fe-Sb(Te,As,Bi,S) oxide. Due to the microscopic size of the particles, it is difficult to determine whether Au belongs to the native reduced form of mustard gold, or is still is part of the complex oxides as it suggested by [14]. This type of mustard gold was often associated with iron antimonates and antimonites, such as tripuhyite $\text{Fe}^{2+}\text{Sb}^{5+}_2\text{O}_6$ or $\text{Fe}^{3+}\text{Sb}^{5+}\text{O}_4$ [21] (Figure 4d). If Au and Ag were assumed to belong to the native phase, then the total of the remaining elements (Table 4) had variable ratios forming a trend towards iron oxides/hydroxides, which was most likely limonite (Figure 5). These compounds were the products of the successive oxidation of tripuhyite.

Table 1. The composition of the primary gold and associated minerals (in wt. %) shown in Figure 2.

No.	Sample	Sp.	Cu	Au	Ag	Bi	Sb	Te	As	Se	S	Total
1	3_3	1	-	98.45	1.86	-	-	-	-	-	-	100.31
2	3_3	2	-	96.23	1.98	-	-	-	-	-	-	98.21
3	3_3	3	41.81	-	0.37	-	19.4	-	6.51	4.64	27.76	100.49
4	3_3	4	-	36.25	-	-	-	49.35	-	5.05	8.6	99.25
5	4_1	1	-	98.54	1.23	-	-	-	-	-	-	99.77
6	4_1	2	-	100.33	1.61	-	-	-	-	-	-	101.94
7	4_1	3	-	35.92	-	-	-	47.67	-	15.35	2.05	100.99
8	4_1	4	-	36.61	-	-	-	48.48	-	11.16	4.29	100.54
9	13_1	1	-	98.1	1.88	-	-	-	-	-	-	99.98
10	13_1	2	1.06	34.8	-	1.28	-	47.35	-	12.24	3.38	100.11
11	13_1	3	-	35.41	-	-	-	45.48	-	15.77	1.03	97.69
12	13_1	4	-	96.05	1.55	-	-	-	-	-	-	97.6
13	13_1	5	-	35.45	-	-	-	45.64	-	14.61	1.71	97.41
14	13_1	6	-	37.41	-	0.92	-	46.47	-	9.91	3.94	98.65
15	13_1	7	0.19	35.58	-	0.75	-	46.39	-	13.28	2.65	98.84
16	13_1	8	0.25	35.26	-	-	-	45.67	-	14.66	1.77	97.61
17	13_1	9	41.89	-	-	-	19.29	-	4.72	4.36	26.97	98.38
18	11_3	1	-	98.52	1.52	-	-	-	-	-	-	100.04
19	11_3	2	-	97.6	1.47	-	-	-	-	-	-	99.07
20	11_3	4	-	35.09	-	0.74	-	45.96	-	14.56	1.32	97.67
21	11_3	5	-	69.91	-	-	-	1.09	-	26.04	2.37	99.41
22	11_3	6	-	35.93	-	-	-	47.78	-	13.6	3.32	100.63
23	11_3	7	-	35.53	-	0.81	-	47.12	-	13.23	2.76	99.45
24	11_3	9	-	37.31	-	0.74	-	46.6	-	10.99	3.84	99.48
25	11_3	10	-	66.71	-	-	-	18.2	-	14.78	-	99.69

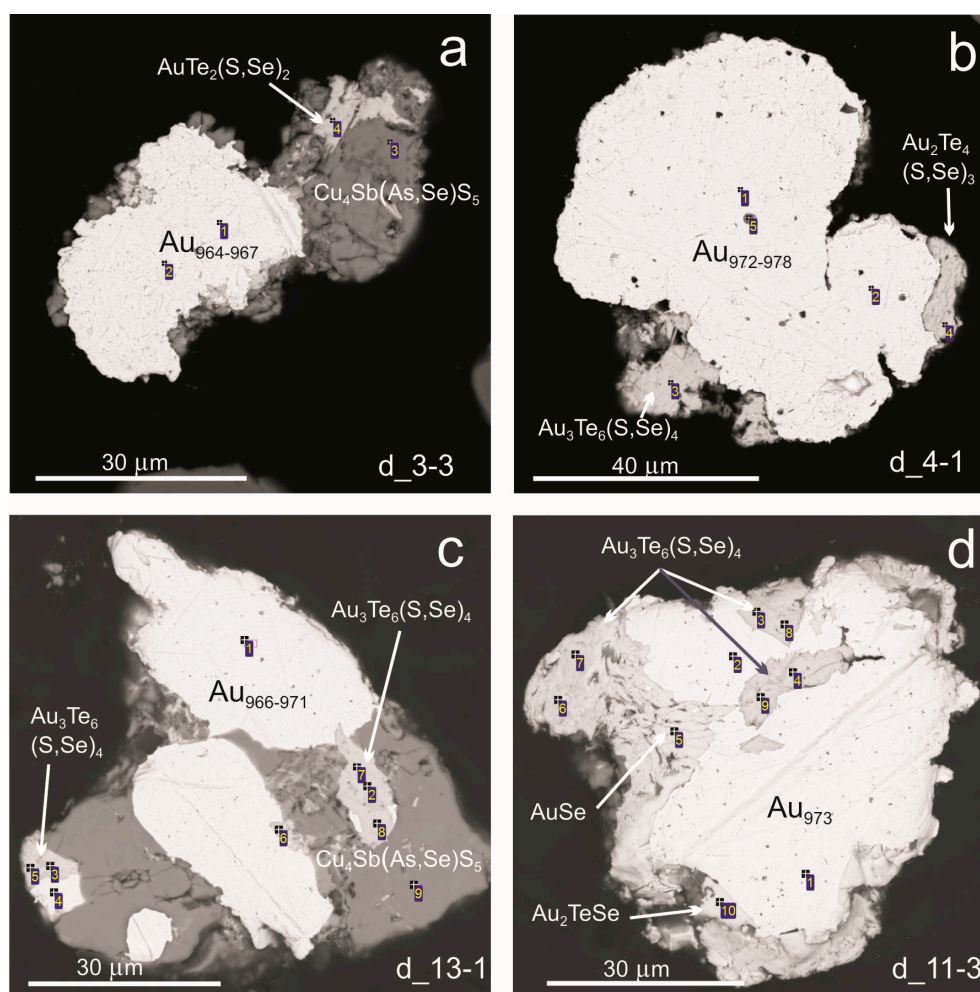


Figure 2. Secondary electron images of scanning electron microscopy (SEM). Primary gold (Au_N , where N is gold fineness) intergrown with the unnamed minerals of Au–Te–Se–S system in an intergrowth with (a)—unnamed phases $Cu_4Sb(As,Se)S_5$ and $AuTe_2(S,Se)_2$; (b)—maletoyvayamite $Au_3Te_6(S,Se)_4$ and unnamed $Au_2Te_4(S,Se)_3$; (c)—unnamed $Cu_4Sb(As,Se)S_5$ and maletoyvayamite; and (d)—maletoyvayamite and unnamed AuSe and Au_2TeSe . Compositions of minerals and unnamed phases shown in Table 1. The numbers in microphotographs are analytical spots, here and in other figures.

Table 2. Formulas to Table 1.

No.	Formula	Abbr.	No.	Formula	Abbr.
1	$Au_{0.97}Ag_{0.03}$	gd	14	$Au_{3.06}Te_{5.87}(Se_{2.02}S_{1.98}Bi_{0.07})_{4.07}$	Mt
2	$Au_{0.97}Ag_{0.03}$	gd	15	$(Au_{2.93}Cu_{0.05})_{2.98}Te_{5.90}(Se_{2.73}S_{1.34}Bi_{0.06})_{4.13}$	Mt
3	$Cu_{3.95}Sb_{0.96}(As_{0.52}Se_{0.35})_{0.87}S_{5.20}$	wt	16	$(Au_{2.98}Cu_{0.07})_{3.05}Te_{5.95}(Se_{3.09}S_{0.92})_{4.01}$	Mt
4	$Au_{1.02}Te_{2.14}(S_{1.48}Se_{0.35})_{1.87}$	unn	17	$Cu_{4.08}Sb_{0.98}(As_{0.39}Se_{0.34})_{0.73}S_{5.21}$	Wt
5	$Au_{0.98}Ag_{0.02}$	gd	18	$Au_{0.97}Ag_{0.03}$	Gd
6	$Au_{0.97}Ag_{0.03}$	gd	19	$Au_{0.97}Ag_{0.03}$	Gd
7	$Au_{2.91}Te_{5.95}(Se_{3.10}S_{1.02})_{4.12}$	mt	20	$Au_{3.02}Te_{6.10}(Se_{3.12}S_{0.70}Bi_{0.06})_{3.88}$	Mt
8	$Au_{1.99}Te_{4.07}(Se_{1.51}S_{1.43})_{2.94}$	unn	21	$Au_{0.93}(Se_{0.86}S_{0.19}Te_{0.02})_{1.07}$	Unn
9	$Au_{0.97}Ag_{0.03}$	gd	22	$Au_{1.97}Te_{4.05}(Se_{1.86}S_{1.12})_{2.98}$	Unn
10	$(Au_{2.76}Cu_{0.26})_{3.02}Te_{5.81}(Se_{2.43}S_{1.65}Bi_{0.10})_{4.18}$	mt	23	$Au_{2.91}Te_{5.95}(Se_{2.70}S_{1.39}Bi_{0.06})_{4.15}$	Mt
11	$Au_{3.04}Te_{6.03}(Se_{3.38}S_{0.54})_{3.92}$	mt	24	$Au_{3.01}Te_{5.81}(Se_{2.21}S_{1.91}Bi_{0.06})_{4.18}$	Mt
12	$Au_{0.97}Ag_{0.03}$	gd	25	$Au_{2.03}Te_{0.85}Se_{1.12}$	Unn
13	$Au_{3.02}Te_{5.99}(Se_{3.10}S_{0.89})_{3.99}$	-	-	-	-

Note. Sp—analysis spot in figures, hereinafter. Signs: gd—gold; wt—watanabeite; mt—maletoyvayamite; and unn—unnamed phase. Abbr.—minerals abbreviation.

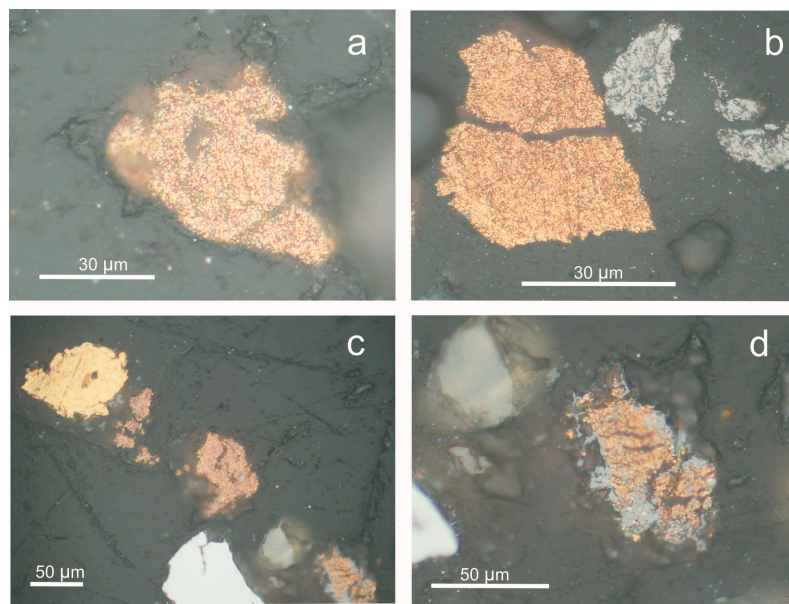


Figure 3. Reflected light photomicrograph of mustard gold (a–c) compared with primary gold (yellow) and pyrite (white) (c) and with Fe–Sb oxide (gray; b,d).

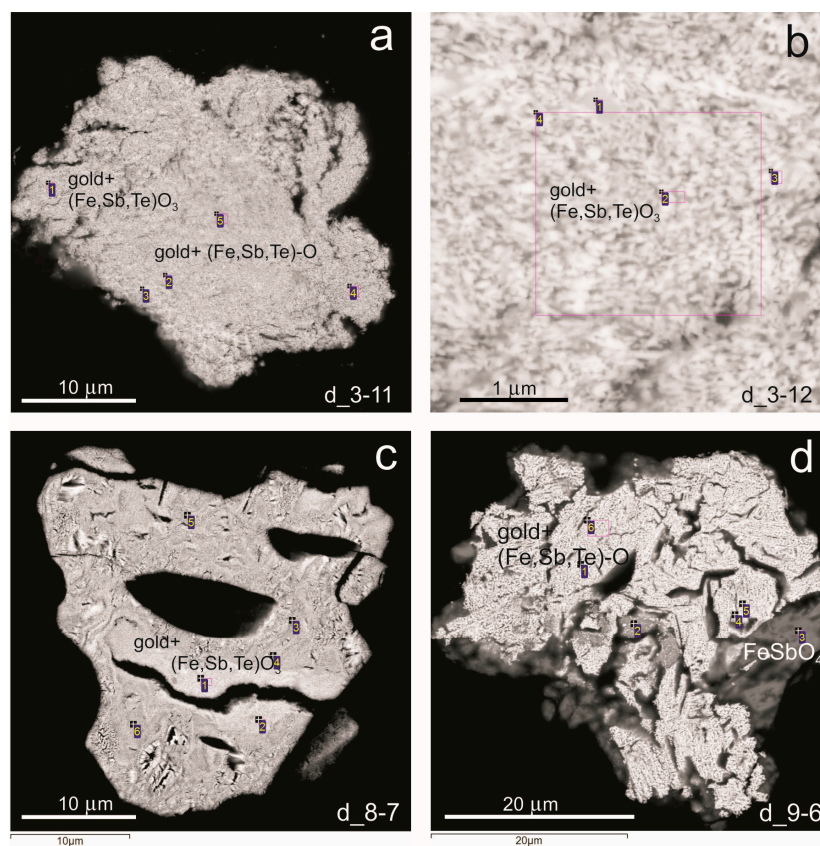


Figure 4. SEM image of mustard (secondary) gold of porous (a,b,d) and colloform (concentrically banded), (c) textural intergrowth with Fe-(Sb,Te,As,Bi,S)-O compounds. The compositions of compounds or mixtures in the analyzed sites are presented in Table 3. d_9-6 spot 3 (FeSbO₄)—tripuhyite. The purple square is scan of analytical area.

Table 3. The mixed compositions of mustard gold and oxides/hydroxides of Fe, Sb, Te, As, Bi, and S (in wt. and at. %) localized in the pores of mustard gold shown in Figure 4.

Sample	Sp.	Fe	Au	Ag	Bi	Sb	Te	As	S	O	Total
3_11	2	5.93	76.70	2.33	-	2.23	2.32	1.40	0.59	7.13	98.63
3_11	3	2.18	88.66	0.70	-	1.00	1.28	0.80	-	5.61	100.23
3_11	4	6.81	78.07	0.84	-	1.13	1.72	0.79	-	9.03	98.39
3_11	5	4.76	79.85	0.78	-	1.69	2.06	1.46	-	9.62	100.22
3_12	2	4.45	82.36	0.72	-	2.12	1.97	1.05	-	6.74	99.41
3_12	4	4.62	81.42	1.00	-	2.16	2.12	0.80	-	6.05	98.17
8_7	1	4.58	70.20	1.40	2.60	9.02	1.00	1.43	0.30	9.42	99.95
8_7	2	5.17	69.63	1.47	2.53	9.58	0.70	1.72	0.39	9.53	100.72
8_7	3	6.63	62.91	1.46	2.02	11.42	1.00	2.28	0.41	12.70	100.83
8_7	4	5.73	67.88	1.32	2.58	10.26	1.21	2.01	0.34	9.57	100.90
8_7	5	6.62	63.82	1.32	2.07	11.11	1.10	2.15	0.35	10.58	99.12
8_7	6	5.44	63.65	1.58	2.72	11.41	1.22	2.06	-	11.85	99.93
9_6	1	5.32	86.15	-	-	-	-	0.63	-	6.66	98.76
9_6	2	15.83	41.44	-	1.53	14.45	1.44	2.06	0.33	23.23	100.31
9_6	4	4.34	85.16	-	-	-	-	-	-	8.78	98.28
9_6	5	1.58	96.52	-	-	-	-	-	-	2.88	100.98
9_6	6	4.39	85.92	-	-	0.70	-	0.61	-	8.80	100.42
Sample	Sp.	Fe	Au	Ag	Bi	Sb	Te	As	S	O	Total
at. %											
3_11	2	9.87	38.18	2.12	-	1.80	1.78	1.83	0.73	43.69	100
3_11	3	4.24	51.55	0.74	-	0.94	1.15	1.22	-	40.16	100
3_11	4	10.34	35.47	0.70	-	0.83	1.21	0.94	-	50.51	100
3_11	5	7.06	35.43	0.63	-	1.21	1.41	1.70	-	52.55	100
3_12	2	7.80	43.18	0.69	-	1.80	1.59	1.45	-	43.50	100
3_12	4	8.48	44.73	1.00	-	1.92	1.80	1.16	-	40.91	100
8_7	1	6.71	30.76	1.12	1.07	6.39	0.68	1.65	0.81	50.81	100
8_7	2	7.42	29.91	1.15	1.02	6.66	0.46	1.94	1.03	50.40	100
8_7	3	8.07	22.92	0.97	0.69	6.73	0.56	2.18	0.92	56.95	100
8_7	4	8.13	28.82	1.02	1.03	7.05	0.79	2.24	0.89	50.02	100
8_7	5	8.92	25.73	0.97	0.79	7.25	0.68	2.28	0.87	52.51	100
8_7	6	7.02	24.58	1.11	0.99	7.13	0.73	2.09	-	56.34	100
9_6	1	9.48	45.93	-	-	0.00	0.00	0.88	-	43.71	100
9_6	2	12.76	9.99	-	0.35	5.64	0.54	1.31	0.49	68.94	100
9_6	4	6.98	40.99	-	-	-	-	-	-	52.03	100
9_6	5	3.85	70.32	-	-	-	-	-	-	25.83	100
9_6	6	6.93	40.59	-	-	0.54	-	0.76	-	51.18	100

Table 4. Compositions (at. %) of oxides/hydroxides of Fe, Sb, Te, As, Bi, and S (after removal of Au and Ag) localized in the pores of mustard gold (data of Table 3 recalculated to 100%).

Sample	Sp.	Fe	Bi	Sb	Te	As	S	O	Total
3_11	2	16.53	-	3.02	2.98	3.07	1.22	73.18	100
3_11	3	8.89	-	1.97	2.41	2.56	-	84.18	100
3_11	4	16.20	-	1.30	1.90	1.47	-	79.13	100
3_11	5	11.04	-	1.89	2.21	2.66	-	82.20	100
3_12	2	13.89	-	3.21	2.83	2.58	-	77.48	100
3_12	4	15.63	-	3.54	3.32	2.14	-	75.38	100
8_7	1	9.85	1.57	9.38	1.00	2.42	1.19	74.59	100
8_7	2	10.76	1.48	9.66	0.67	2.81	1.49	73.12	100
8_7	3	10.60	0.91	8.84	0.74	2.86	1.21	74.84	100
8_7	4	11.59	1.47	10.05	1.13	3.19	1.27	71.30	100
8_7	5	12.17	1.08	9.89	0.93	3.11	1.19	71.64	100
8_7	6	9.45	1.33	9.60	0.98	2.81	-	75.83	100
9_6	1	17.53	-	-	-	1.63	-	80.84	100
9_6	2	14.17	0.39	6.26	0.60	1.46	0.54	76.57	100
9_6	4	11.83	-	-	-	-	-	88.17	100
9_6	5	12.97	-	-	-	-	-	87.03	100
9_6	6	11.66	-	0.91	-	1.28	-	86.15	100

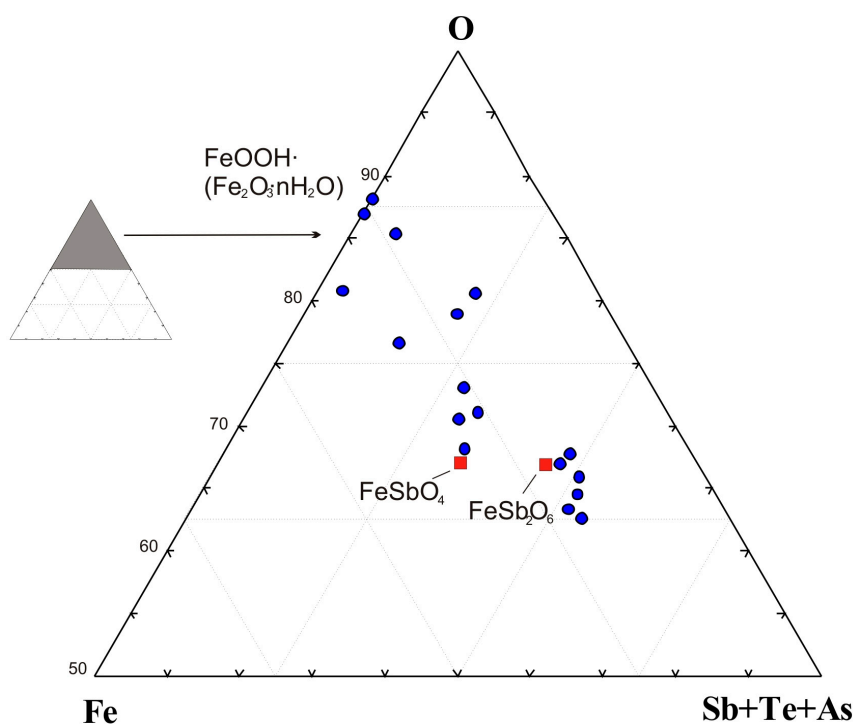


Figure 5. Ternary plot showing the composition of Fe–Sb–Te–As–Se–S-oxides localized in the pores of mustard gold, shown in the Figure 4 and Table 4. FeSbO_4 and FeSb_2O_6 are tripuhyite [21]. The blue circles are analytical data, the red square is stoichiometric composition of minerals.

Less commonly, mustard gold of the Gaching deposit occurred as close intergrowths with goethite/hydrogoethite/limonite, forming different colloform and spotted textures (Figure 6a,b). Goethite also sometimes formed a rims on mustard gold microaggregates (Figure 6c,d). Mustard gold was high fineness in this case and did not contain Ag. The presence of iron in the gold was the result of the imposition of Fe hydroxides during the analytical procedure (Table 5). Association of secondary gold and Fe hydroxides was the final oxidation product of the studied parageneses. Secondary high fineness gold in association with supergene minerals, including goethite, has been described in Au-bearing regolith in deposits in Kazakhstan [22], where the secondary gold is not the mustard species, but has a crystal shape and different genesis.

Table 5. The mixed compositions of mustard gold and goethite/hydrogoethite (wt. %) as shown in Figure 6.

No.	Sample	Sp.	Fe	Au	O	Total
1	3_1	1	-	97.18	-	97.18
2	3_1	2	-	97.62	-	97.62
3	3_1	3	52.57	-	45.39	97.96
4	4_1	1	-	98.62	-	98.62
5	4_1	2	13.26	77.8	9.65	100.71
6	4_1	3	51.19	0.92	45.18	97.29
7	4_2	1	4.95	90.18	3.99	99.12
8	4_5	11	-	97.57	-	97.57
9	4_5	2	14.11	70.06	17.48	101.65
10	4-5a	1	12.87	72.42	15.28	100.57
11	4-5a	2	12.18	72.23	16.12	100.53
12	4-5a	3	13.14	71.36	16.06	100.56

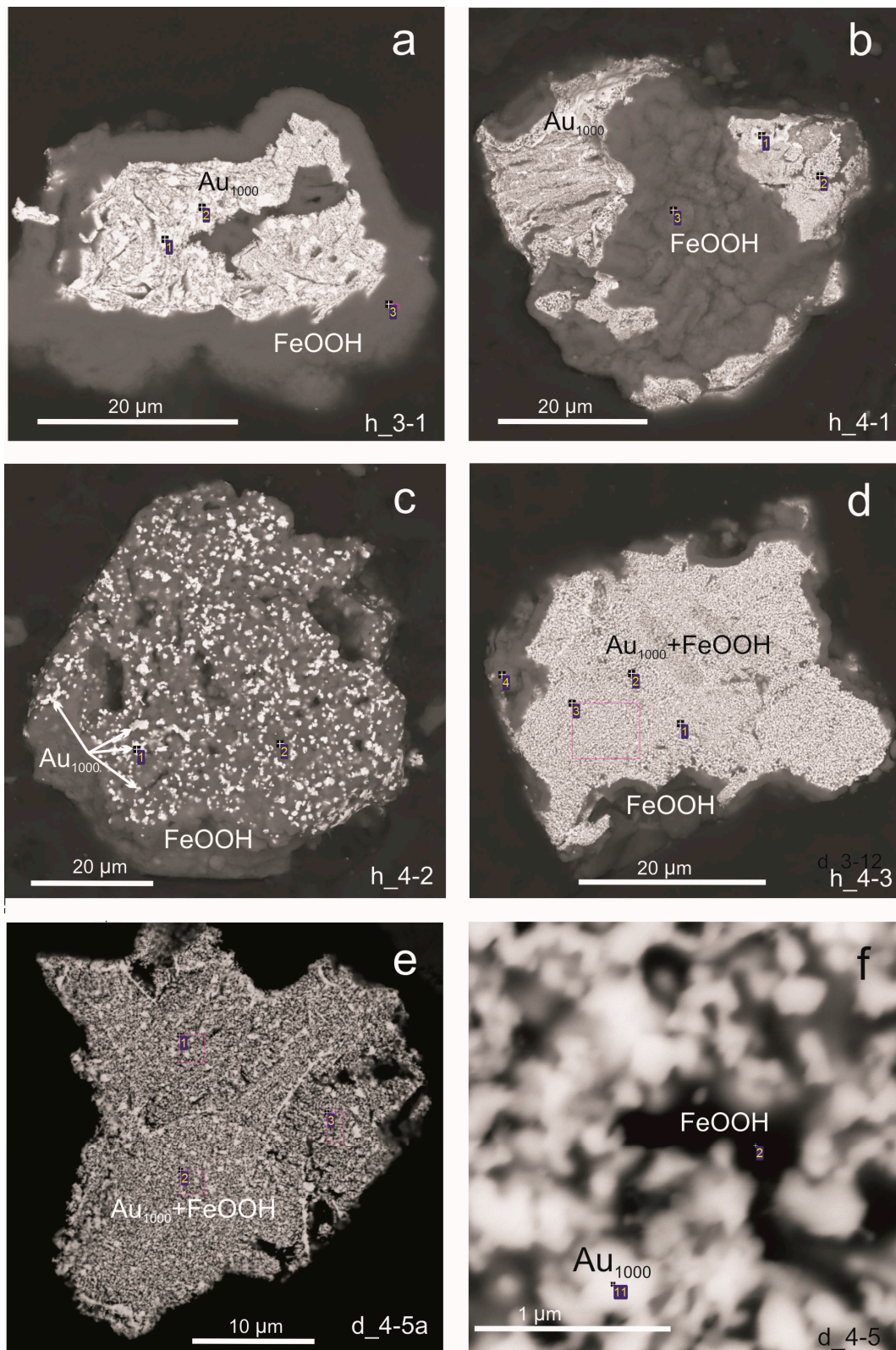


Figure 6. SEM image of mustard gold of colloform (a,b) and spotted (c–f) textures intergrown with goethite/hydrogoethite/limonite (FeOOH). The compositions of compounds and mixtures of the minerals are presented in Table 5. The purple square is scan analytical area.

3.2. Transformation Sequence from Calaverite to Gold

In addition Au–Te–Se–S system minerals and gold (primary and mustard), multicomponent grains were found that show the individual stages of the formation of mustard gold from calaverite (Figure 7). These grains had a vermicular texture, where secondary Fe–Sb–Te oxides with worm-like shapes developed in a matrix of calaverite. The smallest particles of gold were deposited in the marginal zones of these oxides (Figure 7, Table 6). All compositions of AuTe_2 relate to calaverite, since the concentration of Ag in these minerals did not exceed the 3.4 wt. % [23]. Krennerite $(\text{Au,Ag})\text{Te}_2$ was not detected in the ore assemblage. At the same time, maletoyvayamite intergrown with calaverite did not undergo dissolution (Figure 7c,d). Calaverite was the Au-bearing mineral that oxidized due to reaction with infiltrating fluids containing Fe, Sb \pm As, Se, S, Bi, along with the formation of secondary minerals (complex Au oxides, Fe antimonates, and stibiotellurates in the first stage and goethite/hydrogoetite in the final supergene stage).

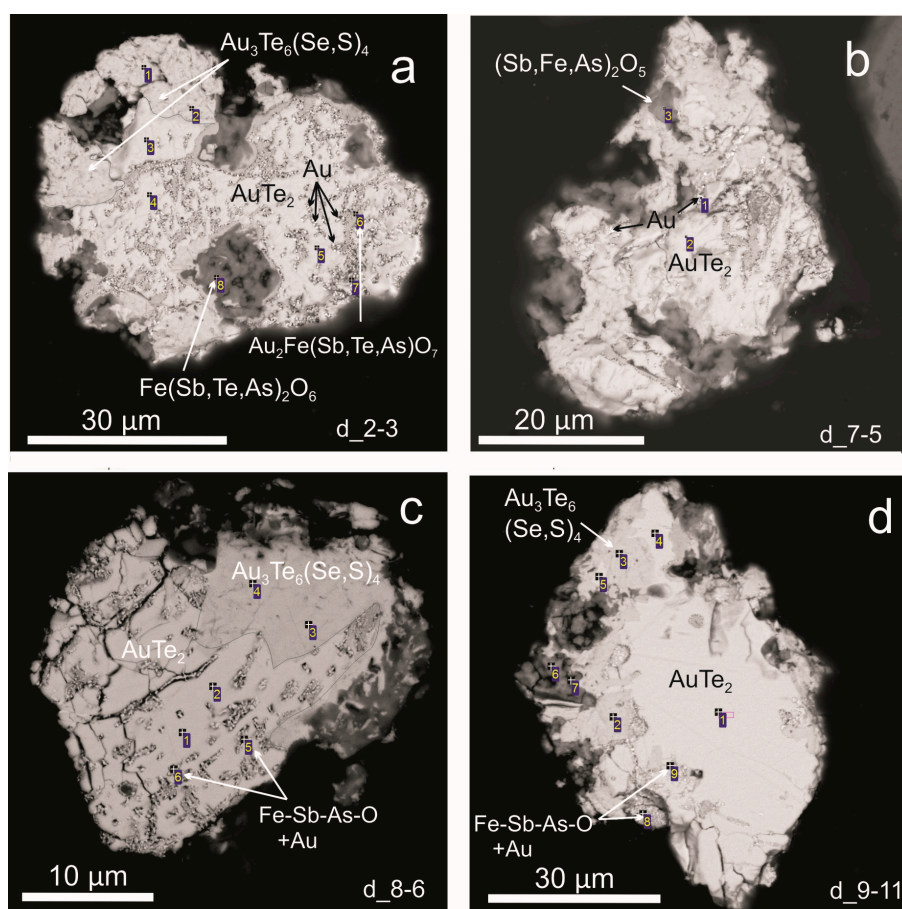


Figure 7. SEM images showing the reacted calaverite grains, the surface of microporous gold (a–d), and boundary between microporous gold and calaverite (a–d). AuTe_2 —calaverite, $\text{Au}_3\text{Te}_6(\text{Se,S})_4$ —maletoyvayamite, and $\text{Fe}(\text{Sb,Te,As})_2\text{O}_6$ —tripuhyite. 1–9—the compositions of compounds or mixtures in the analyzed spots are presented in Table 6.

All analyses of mustard gold from the various samples (Figures 4 and 6–8) on the diagram O–Fe + Sb + As + Te + Se + S–Au (+Ag) were located along the line connecting the $(\text{Fe,Sb,As,Te,Se,S})\text{O}_3$ and native gold, possibly showing the ratio of particles of fine gold and the matrix of Fe–Sb oxides (Trend I; Figure 9). The concentration of Fe varied greatly in these compounds and was not correlated with the sum of Sb, As, Te, Se, and S. This indicates that Fe,Sb \pm As,Te,Se,S oxides (tripuhyite) were in turn also successively oxidized and contain hydroxides in the compound (Figure 5).

Table 6. Composition of calaverite grains, products of its replacement (mustard gold and Fe antimonate/tellurate) and associated minerals (maletoyvayamite) (wt. %) shown in Figure 7.

Sample	Sp.	Fe	Au	Ag	Sb	Te	As	Se	S	O	Total	Abbr.	Formula
2_3	1	-	35.25	-	-	45.61	-	16.63	0.34	-	97.83	mt	$Au_{3.07}Te_{6.13}(Se_{3.61}S_{0.18})_{3.79}$
2_3	2	-	35.32	-	-	46.06	-	16.32	1.13	-	98.83	mt	$Au_{2.98}Te_{6.00}(Se_{3.44}S_{0.59})_{4.03}$
2_3	3	-	43.52	0.41	-	52.91	-	1.52	-	-	98.36	calv	$(Au_{1.01}Ag_{0.02})_{1.03}(Te_{1.89}Se_{0.09})_{1.98}$
2_3	4	-	44.79	0.37	-	53.38	-	1.67	-	-	100.21	calv	$(Au_{1.02}Ag_{0.02})_{1.04}(Te_{1.87}Se_{0.09})_{1.96}$
2_3	5	-	43.88	-	-	51.97	-	1.4	0.27	-	97.52	calv	$Au_{1.02}(Te_{1.86}Se_{0.08}S_{0.04})_{1.98}$
2_3	6	6.62	59.19	0.96	10.1	3.53	2.43	-	-	15.71	98.54	Auox	$(Au_{0.97}Ag_{0.03})_{1.00}(Fe_{0.36}Sb_{0.27}Te_{0.10}As_{0.10})_{0.83}O_{3.17}$
7_5	2	-	44.7	-	-	53.45	-	1.77	0.68	-	100.6	calv	$Au_{0.99}(Te_{1.82}Se_{0.10}S_{0.09})_{2.01}$
8_6	1	-	42.55	0.97	-	54.36	-	1.87	0.22	-	99.97	calv	$(Au_{0.95}Ag_{0.04})_{0.99}(Te_{1.88}Se_{0.10}S_{0.03})_{2.01}$
8_6	2	-	41.26	0.82	-	54.5	-	1.93	0.27	-	98.78	calv	$(Au_{0.93}Ag_{0.03})_{0.96}(Te_{1.89}Se_{0.11}S_{0.04})_{2.04}$
8_6	3	-	36.46	-	-	46.71	-	14.44	1.99	-	99.6	mt	$Au_{3.02}Te_{5.98}(Se_{2.99}S_{1.01})_{4.00}$
8_6	4	-	37.39	-	-	46.89	-	10.37	3.83	-	98.48	mt	$Au_{3.05}Te_{5.91}(Se_{2.11}S_{1.92})_{4.03}$
8_6	5	2.64	53.84	-	2.36	29.31	0.73	0.46	-	8.96	98.30	Auox	$Au_{0.96}(Te_{0.80}Fe_{0.16}Sb_{0.07}As_{0.03}Se_{0.02})_{1.08}O_{1.96}$
8_6	6	1.98	58.09	0.85	1.41	30.09	0.43	0.64	-	6.51	100.00	Auox	$(Au_{2.94}Ag_{0.08})_{3.02}(Te_{2.35}Fe_{0.33}Sb_{0.12}Se_{0.08}As_{0.06})_{2.94}O_{4.05}$
9_11	1	-	42.58	-	-	54.27	-	1.61	-	-	98.46	calv	$Au_{0.98}(Te_{1.93}Se_{0.09})_{2.02}$
9_11	2	-	35.92	-	-	46.06	-	18.08	-	-	100.06	mt	$Au_{3.07}Te_{6.08}Se_{3.85}$
9_11	3	-	35.24	-	-	45.54	-	17.6	-	-	98.38	mt	$Au_{3.07}Te_{6.12}Se_{3.82}$
9_11	4	-	42.98	-	-	54.27	-	1.68	-	-	98.93	calv	$Au_{0.98}(Te_{1.92}Se_{0.10})_{2.02}$
9_11	5	0.42	42.15	-	-	53.94	-	1.64	-	-	98.15	calv	$Au_{0.97}(Te_{1.91}Se_{0.09}Fe_{0.03})_{2.03}$

Note. Auox—complex Au-antimonates and Au-tellurates, mt—maletoyvayamite, and calv—calaverite. Abbr.—minerals abbreviation.

Table 7. Compositions of Au-(Te,Fe,Se,Sb,Bi,S,As) and Sb-(Fe,Te,As,S,Au,Ag) oxides, maletoyvayamite and calaverite (in wt %) shown in Figure 8.

Sample	Sp.	Fe	Au	Ag	Bi	Sb	Te	As	Se	S	O	Total	Abbr.	Formula
8_10	1	4.36	56.34	2.3	-	5.72	11.92	1.58	5.06	1.74	10.53	99.55	Auox	(Au _{0.87} Ag _{0.06}) _{0.93} (Te _{0.28} Fe _{0.22} Se _{0.19} S _{0.16} Sb _{0.14} As _{0.06}) _{0.99} O _{2.00}
8_10	2	2.91	55.94	2.62	1.58	6.11	13.67	-	5.36	2.03	9.68	99.9	Auox	(Au _{0.90} Ag _{0.08}) _{0.98} (Te _{0.34} Se _{0.22} S _{0.20} Fe _{0.16} Sb _{0.16} Bi _{0.02}) _{1.10} O _{1.92}
8_10	3	3.92	59.55	2.24	0.92	4.61	8.19	0.94	3.03	1.3	9.23	93.93	Auox	(Au _{1.04} Ag _{0.07}) _{1.11} (Fe _{0.23} Te _{0.22} S _{0.14} Sb _{0.13} As _{0.04} Bi _{0.02}) _{0.91} O _{1.98}
8_10	4	2.15	74.83	1.67	1.77	5.34	1.31	-	-	1.78	10.11	98.96	Auox	(Au _{1.29} Ag _{0.05}) _{1.34} (S _{0.19} Sb _{0.15} Fe _{0.12} Te _{0.03} Bi _{0.03}) _{0.52} O _{2.14}
8_10	5	2.71	54.62	2.97	1.5	3.59	17.25	-	6.96	1.91	7.51	99.02	Auox	(Au _{0.97} Ag _{0.10}) _{1.07} (Te _{0.47} Se _{0.31} S _{0.21} Fe _{0.16} Sb _{0.10} Bi _{0.03}) _{1.28} O _{1.65}
8_10	6	2.17	78.16	1.02	1.68	4.56	1.10	-	-	1.47	7.6	97.76	Auox	(Au _{1.56} Ag _{0.04}) _{1.60} (S _{0.18} Sb _{0.15} Fe _{0.14} Te _{0.03} Bi _{0.03}) _{0.53} O _{1.87}
8_10	9	6.26	2.37	0.48	-	45.52	5.30	0.91	-	-	24.37	85.21	SbFeox	(Sb _{0.72} Fe _{0.20} Te _{0.08} As _{0.02} Au _{0.02} Ag _{0.01}) _{1.05} O _{2.94}
8_11	1	4.11	52.68	1.99	1.54	5.64	12.35	1.19	4.88	1.12	9.3	94.8	Auox	(Au _{0.89} Ag _{0.06}) _{0.95} (Te _{0.32} Fe _{0.23} Se _{0.21} Sb _{0.15} S _{0.12} As _{0.05} Bi _{0.02}) _{1.10} O _{1.94}
8_11	2	4.12	54.54	2.64	1.94	5.81	13.8	1.28	6.25	1.61	8.89	100.88	Auox	(Au _{0.89} Ag _{0.08}) _{0.97} (Te _{0.35} Se _{0.26} Fe _{0.23} S _{0.16} Sb _{0.15} As _{0.06} Bi _{0.03}) _{1.24} O _{1.79}
8_11	3	4.23	53.55	2.50	1.98	5.8	11.84	1.58	5.39	1.31	9.25	97.43	Auox	(Au _{0.89} Ag _{0.08}) _{0.97} (Te _{0.35} Se _{0.26} Fe _{0.23} S _{0.16} Sb _{0.15} As _{0.06} Bi _{0.03}) _{1.24} O _{1.79}
8_11	4	4.25	58.63	2.38	2.08	4.61	9.70	1.48	4.42	1.4	8.28	97.23	Auox	(Au _{1.03} Ag _{0.08}) _{1.11} (Te _{0.26} Fe _{0.25} Se _{0.19} S _{0.15} Sb _{0.13} As _{0.07} Bi _{0.03}) _{1.08} O _{1.80}
8_11	5	2.71	50.98	2.39	1.51	2.9	20.88	0.98	8.59	1.91	5.89	98.74	Auox	(Au _{0.97} Ag _{0.08}) _{1.05} (Te _{0.61} Se _{0.41} S _{0.22} Fe _{0.17} Sb _{0.09} As _{0.05} Bi _{0.03}) _{1.58} O _{1.37}
8_11	6	4.03	53.89	1.99	1.85	4.24	15.25	1.19	6.73	1.34	7.05	97.56	Auox	(Au _{0.99} Ag _{0.07}) _{1.06} (Te _{0.43} Se _{0.31} Fe _{0.25} S _{0.15} Sb _{0.13} As _{0.06} Bi _{0.03}) _{1.36} O _{1.59}
8_11	7	4.47	53.75	1.42	2.07	7.21	12.97	1.37	5.63	1.45	9.03	99.37	Auox	(Au _{0.89} Ag _{0.04}) _{0.93} (Te _{0.33} Fe _{0.25} Se _{0.23} Sb _{0.19} S _{0.15} As _{0.06} Bi _{0.03}) _{1.24} O _{1.83}
8_11	8	6.22	5.33	1.49	-	51.14	6.38	0.91	-	0.18	26.66	98.31	SbFeox	(Sb _{0.73} Fe _{0.18} Te _{0.09} As _{0.02} S _{0.01} Au _{0.05} Ag _{0.02}) _{1.10} O _{2.90}
11_7	1	6.93	58.62	1.37	-	12.92	1.74	2.13	-	-	14.17	97.88	Auox	(Au _{1.02} Ag _{0.04}) _{1.06} (Fe _{0.40} Sb _{0.36} As _{0.10} Te _{0.05}) _{0.91} O _{3.03}
11_7	2	6.30	58.55	1.38	-	13.36	1.57	2.14	-	-	13.26	96.56	Auox	(Au _{1.06} Ag _{0.05}) _{1.11} (Sb _{0.39} Fe _{0.38} As _{0.10} Te _{0.04}) _{0.92} O _{2.97}
11_7	3	-	35.55	-	1.19	-	47.63	-	10.4	5.41	-	100.18	mt	Au _{2.73} Te _{5.64} (S _{2.55} Se _{1.99} Bi _{0.09}) _{4.63}
11_7	4	-	36.77	-	0.74	-	47.39	-	7.92	4.89	-	97.71	mt	Au _{2.98} Te _{5.93} (S _{2.43} Se _{1.60} Bi _{0.06}) _{4.09}
11_7	5	-	41.95	-	-	-	53.77	-	1.21	-	-	96.93	calv	Au _{0.98} (Te _{1.95} Se _{0.07}) _{2.02}
11_7	6	-	44.06	-	-	-	54.28	-	1.16	-	-	99.50	calv	Au _{1.01} (Te _{1.92} Se _{0.07}) _{1.99}

Note. Auox—complex Au-antimonates/tellurates, SbFeox—Fe-antimonite, mt—maletoyvayamite, and calv—calaverite. Abbr.—minerals abbreviation.

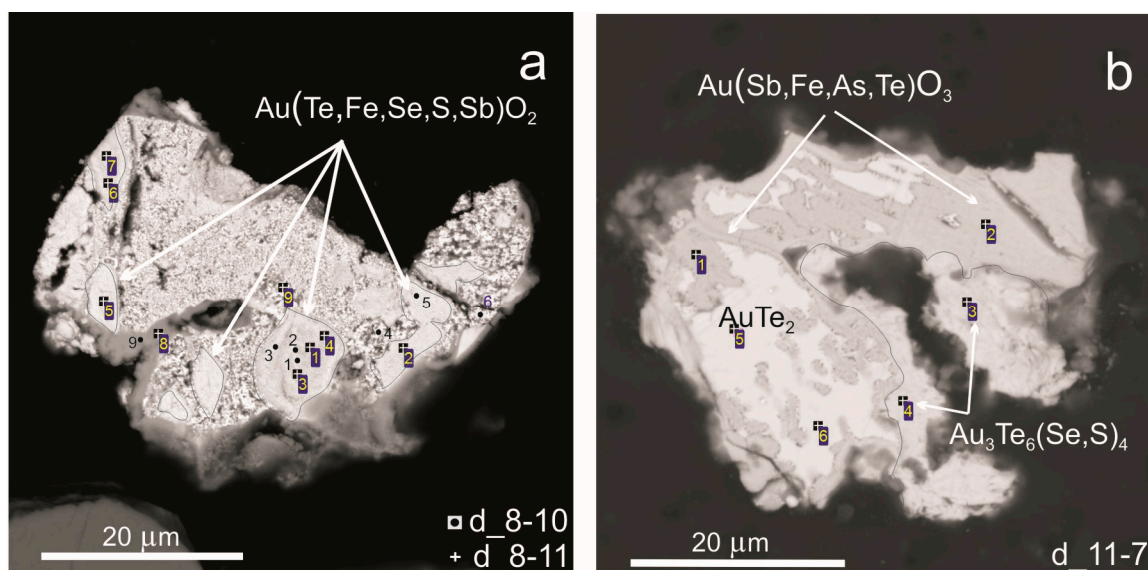


Figure 8. SEM images of complex oxides: zonal Au tellurates in association with mustard gold (a) and homogeneous Fe-rich auroantimonate $\text{Au}(\text{Sb,Fe,As,Te})\text{O}_3$ in association with calaverite (AuTe_2) and maletoyvayamite ($\text{Au}_3\text{Te}_6(\text{Se,S})_4$) (b). 1–11—the compositions of compounds or mixtures in the analyzed sites are presented in Table 7.

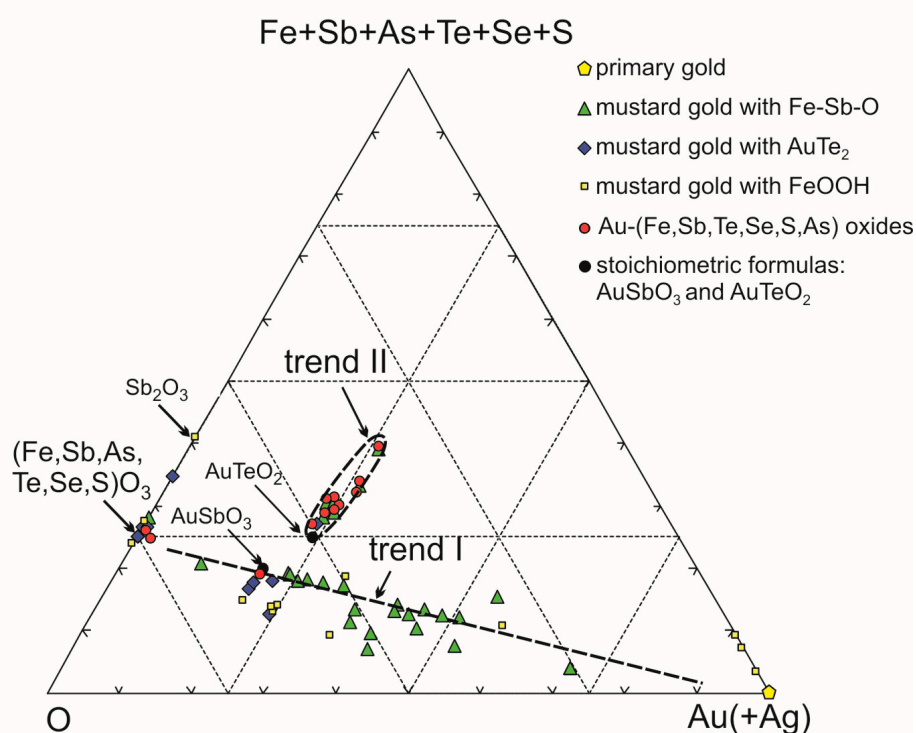


Figure 9. The composition of mustard gold mixed with Fe–Sb–Te–As–Se–S-oxide matrix (trend I) and Au-complex oxides (trend II) in O–Fe + Sb + As + Te + Se + S–Au (+Ag) diagram from the various associations shown in the Figures 2, 4 and 6–8.

The part of the analyses that correspond to homogeneous areas of mineral microaggregates (Figure 8) formed another compositional trend (Trend II), where the concentration of Au remained approximately constant, while the ratio of oxygen to the sum of Sb, As, Te, Se, and S (chalcogenides) varied within certain limits (Figure 9). The composition with the maximum amount of oxygen in this trend corresponded to the formulae $\text{Au}(\text{Te,Fe,Se,Sb,S,As})\text{O}_3$ and $\text{Au}(\text{Fe,Sb})\text{O}_3$ (Figure 9) with variable

ratios of chalcogenides and Fe. These probably exist as chemical compounds rather than as mixtures of gold and Fe tellurate/antimonate. The existence of auroantimonate or Au–Sb-oxides in natural systems is highly questionable according to [24]. However, it is difficult to agree that the numerous compositions located along trend II were mixtures of gold and oxides, since the concentration of Au remained almost constant in different spots of the grains (Figure 9). The gray-zoned areas of these Au oxides (Figure 8a) were due to the different degrees of oxidation of tellurium, antimony, and other elements structurally related to Au. The Au, Sb-oxides, and auroantimonate were described by [25–27] also.

4. Discussion

Mustard gold is characteristic in gold-telluride deposits [9,10], antimony-gold deposits [11,12,24,28], and laterites [7,8]. The stibian mustard gold from the Kriván Au deposit, which formed from Au₂Sb is a composite material consisting of submicroporous sponge of gold with pores infilled by oxidation products of Sb and Fe [24]. In contrast, the Krásná Hora deposit (Czech Republic) a reverse reaction is observed in the formation of aurostibite to gold via dissolution-precipitation and solid-state diffusion processes at temperatures <200 °C [29]. In all cases the formation of mustard gold occurred due to the decomposition of tellurides, antimonides, sulphides, bismuthides of Au(Ag), and low-grade gold under oxidation conditions. Since the Gaching deposit is gold-telluride, the transformation mechanism of Au telluride (calaverite) is important to reconstruct. It is likely that there were two mechanisms for the replacement of primary Au tellurides with different oxidation intensities and different degrees of removal of Te:

- (1) $\text{AuTe}_2 + \text{Fe, Sb, Bi, As, Se, and S-containing solutions} + \text{O}_2 \rightarrow \text{Au} + \text{Te,Se solid solution} + \text{TeO}_2 + \text{Fe(Sb,As)O}_3$ as a composite of a gold sponge and Sb–Fe oxide \pm admixtures.
- (2) $\text{AuTe}_2 + \text{Fe, Sb, Bi, As, Se, and S-containing solutions} + \text{O}_2 \rightarrow \text{Au(Te,Fe,Se,Sb,S)O}_2$.

The appearance of secondary high-grade mustard gold and tellurites/tellurates in the Aginskoye deposit (Kamchatka) [4,5] and placer region of Northeast Russia [8] are considered to be products of hypogene processes. Alternatively, mustard gold, Au antimonates/tellurates, and complex oxides of Au are products of hypogene processes [3,24] that formed from hydrothermal low-temperature solutions at a high oxidative potential.

Moreover, the auroantimonate (AuSbO₃) that was found by Z. Johan and co-authors [27] in Au–Sb ores of the Krásná Hora gold deposit and by G.N. Gamyagin and co-authors [25] in Eastern Yakutia was characterized in detail by I.Ya Nekrasov [3], who obtained the compositions and X-ray images of this oxide. Our data confirmed the presence of Au oxides in the epithermal Gaching deposit, however, there are doubts regarding its existence [24]. It remains stable in hypogene conditions, but it is not stable in the hypergenesis zone, where it decomposes into sponge gold and antimony oxides, therefore, it is rarely found in nature [3].

Experimental studies by [29,30] have identified a diversity of reactionary textures and the transition mechanism of calaverite (AuTe₂) into metallic gold. During the replacement of calaverite by gold, there is the coupled calaverite dissolution-gold (re)precipitation (ICDR) mechanism [29,30]. This is a redox reaction controlled by the solution chemistry. The rate of replacement would be controlled by such major factors: The pH value, redox, and temperature. Natural mustard gold, which results from the weathering of Au-tellurides, may form via a similar dissolution-reprecipitation mechanism. It has been shown that the replacement of krennerite/calaverite by gold occurs only in hydrothermal solutions, whereas such reactions do not occur in anhydrous conditions [31]. These minerals follow a simple ICDR reaction path leading to pseudomorphic replacement by gold; and both minerals transform at similar rates. The presence of Ag in tellurides has an effect on the ICDR reaction path, since the solid-state reactions in the transformation of sylvanite (Au,Ag)₂Te₄ is also involved. The porosity is textural evidence for a CDR reaction, which leads to the negative volume changes [32]. The reaction is sustained by continuous mass transport through open pathways allowing the influx of

Fe,Sb,As,Se,Bi-solutes and the removal of oxidized Te from the reaction interface. Au(I) is controlled by the redox potential of the fluid at the reaction front. The decrease in oxygen activity favors the precipitation of gold since the oxygen is continuously removed as Te(IV) complexes by the oxidation of tellurium, and the soluble oxidation product leaves the reaction front by mass transport in the fluid, and precipitates far from the site of dissolution [31]. The dominant Te aqueous species is $\text{H}_2\text{TeO}_3(\text{aq})$, which occurs under acidic to slightly basic (pH 2–7) conditions [33]. In low-sulfidation environments, telluride and native tellurium deposition may result from condensation of $\text{H}_2\text{Te}(\text{g})$ and $\text{Te}_2(\text{g})$ into saline waters. A minor amount of tellurium will be deposited by cooling or fluid mixing [34]. Native tellurium and tellurium-selenium solid solutions precipitate out of the mustard gold grains as separate grains or in intergrowths with the maletoyvayamite [14,19].

Microaggregates of mustard gold can be large in size, but they are unstable in the hypergenic process due to the loose texture and therefore have weak placer-forming potential. The concentration of Au increased from large size fractions to small ones, and its greatest value was reached in the finest grain concentrates (Figure 10). This circumstance requires attention when developing technological schemes for exploiting such deposits and explains the discrepancy between high concentrations of Au in samples and the absence (or undetected) of its mineral forms.

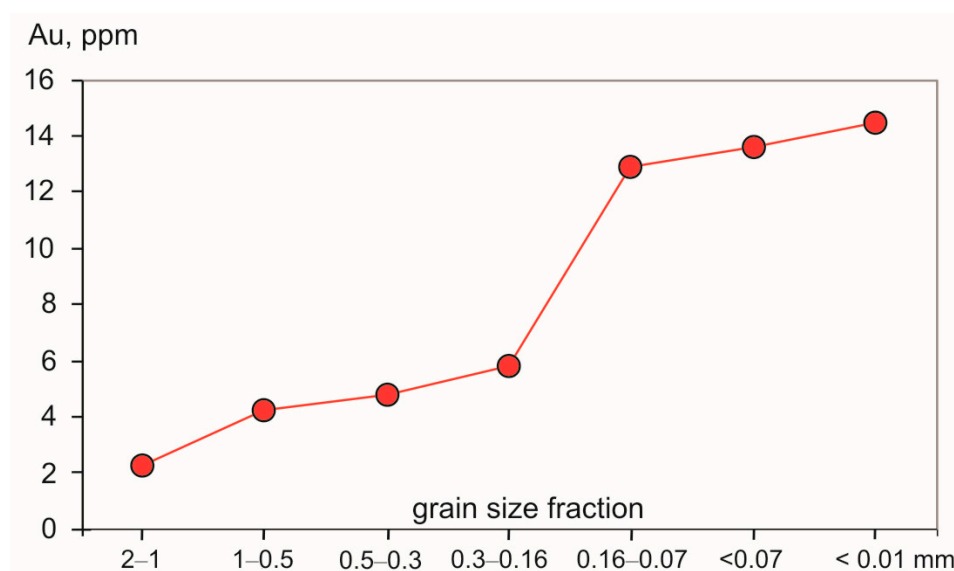


Figure 10. The graph of increasing Au concentration with decreasing size fraction of rock crushing.

Au(Ag) tellurides in gold deposits are considered refractory ores from a mineral processing perspective, as they are not efficiently leachable in cyanide solutions. Typically, tellurides are heated at temperatures ≥ 800 °C [35,36]. Au tellurides under hydrothermal conditions can be transformed into gold relatively fast (within hours) under all conditions at ~ 200 °C. This process can be used in preliminary ore processing before the addition cyanide instead of the toxic process of ore heating. This method has an advantage, as the dissolution of a gold telluride occurs over a wider range of solution conditions than Au–Ag alloys [31]. Porous gold obtained by the replacement of Au tellurides can present significant technological potential due to its low density, high strength and large surface area [33].

5. Conclusions

Gold in the epithermal Au–Ag Gaching deposit is present as primary gold (fineness 964‰–978‰) occurring as intergrowths with a numerous minerals (maletoyvayamite $\text{Au}_3\text{Te}_6\text{Se}_4$ and other rare unnamed phases of Au–Te–Se–S system), and as secondary porous mustard gold of fineness 1000‰.

There are two types of mustard gold:

- (a) Mustard gold with inclusions of the oxides of Sb, Te(Se,S), and Fe (Fe-antimonate/tellurate) infilling the pores of spongy gold—the early (hypogene) transformation stage of calaverite due to the impact of Fe, Sb, Te, As, Se, and S-containing hydrothermal solutions and high oxidation potential.
- (b) Spotted and colloform gold consisting of aggregates of small particles of gold in a goethite/hydrogoethite matrix—the late (possibly hypergene) transformation stage associated with the maximum degree of ore oxidation.

Among the numerous compounds of Au, only calaverite was oxidized and transformed into mustard gold. The other minerals (Au sulfoselenotelluride—maletiyvayamite) remained unchanged. This process is associated with hypogene conditions and proceeds in two directions: (a) Formation of a mixture of Fe–Sb oxides (tripuhyite) and gold particles, and (b) formation of Au–Sb(Te,Se,S,As) oxides by calaverite.

Mustard gold has a weak placer-forming potential in hypergene conditions because it disintegrates easily into dust particles that enrich the fine fractions of oxidized ores.

Author Contributions: N.D.T. conceived and designed the study, interpreted the results, and wrote this article. G.A.P. provided valuable ideas for the discussion and edited the manuscript. O.V.B. provided samples for research and determined the Au concentrations in rock fractions. E.G.S. provided the field work on the gold ore occurrences.

Funding: The studies were carried out within the framework of the state assignment of the VS Sobolev Institute of Geology and Mineralogy of Siberian Branch of Russian Academy of Sciences financed by Ministry of Science and Higher Education of the Russian Federation. Financial assistance from the Russian Foundation of Basic Research projects No 19-05-00316.

Acknowledgments: The authors thank N. Karmanov, M. Khlestov and V. Danilovskaya for help in carrying out a large amount of work on a scanning electron microscope and an X-ray spectral microanalyzer (VS Sobolev Institute of Geology and Mineralogy, Siberian Branch, Russian Academy of Sciences).

Conflicts of Interest: The authors declare no conflict of interest.

References

1. Lindgren, W. *Mineral Deposits*; McGraw-Hill Book Company, Inc.: New York, NY, USA; London, UK, 1933; p. 930.
2. Sotnikov, V.I. Gold in the bedrock source—Placer system. *Soros Educ. J.* **1998**, *5*, 66–71. (In Russian)
3. Nekrasov, I.Y. *Geochemistry, Mineralogy and Genesis of Gold Deposits*; Nauka: Moscow, Russia, 1991; p. 302. (In Russian)
4. Okrugin, V.M.; Andreeva, E.D.; Yablokova, D.A.; Okrugina, A.M.; Chubarov, V.M.; Ananiev, V.V. The new data on the ores of the Aginskoye gold-telluride deposit (Central Kamchatka). In *“Volcanism and Its Associated Processes” Conference*; Petropavlovsk-Kamchatsky: Kamchatka Krai, Russia, 2014; pp. 335–341. (In Russian)
5. Okrugin, V.M.; Andreeva, E.; Etschmann, B.; Pring, A.; Li, K.; Zhao, J.; Griffiths, G.; Lumpkin, G.R.; Triani, G.; Brugger, J. Microporous gold: Comparison of textures from Nature and experiments. *Am. Mineral.* **2014**, *99*, 1171–1174. [[CrossRef](#)]
6. Kudaeva, A.L.; Andreeva, E.D. Mustard gold: Characteristics, types and chemical composition. In *The Natural Environment of Kamchatka*; Petropavlovsk-Kamchatsky: Kamchatka Krai, Russia, 2014; pp. 17–29. (In Russian)
7. Wilson, A.F. Origin of quartz-free gold nuggets and supergene gold found in laterites and soils—A review and some new observations. *Aust. J. Earth Sci.* **1984**, *31*, 303–316.
8. Litvinenko, I.S.; Shilina, L.A. Hypergene gold neomineralization in placer deposits of Nizhne-Myakitsky ore-placer field, North-East Russia. *J. Ores Met.* **2017**, *1*, 75–90. (In Russian)
9. Petersen, S.O.; Makovicky, E.; Juiling, L.; Rose-Hansen, J. Mustard gold from the Dongping Au-Te deposit, Hebei province, People’s Republic of China. *N. Jb. Mineral. Mh.* **1999**, *8*, 337–357.
10. Li, J.; Makovicky, E. New studies on mustard gold from the Dongping Mines, Hebei Province, China: The tellurian, plumbian, manganoan and mixed varieties. *N. Jb. Mineral. Abh.* **2001**, *176*, 269–297.
11. Gamyandin, G.N.; Zhdanov, Y.Y.; Nekrasov, T.Y.; Leskova, N.V. “Mustard” gold from gold-antimony ores of Eastern Yakutia. *New Data Miner.* **1987**, *34*, 13–20. (In Russian)

12. Dill, H.G.; Weiser, T.; Benhardt, I.R.; Kilibarda, R. The composite gold—Antimony vein deposit at Kharma (Bolivia). *Econ. Geol.* **1995**, *90*, 51–66. [[CrossRef](#)]
13. Wang, D.; Liu, J.; Zhai, D.; Carranza, E.J.M.; Wang, Y.; Zhen, S.; Wang, J.; Wang, J.; Liu, Z.; Zhang, F. Mineral Paragenesis and Ore-Forming Processes of the Dongping Gold Deposit, Hebei Province, China. *Resour. Geol.* **2019**, *29*, 287–313. [[CrossRef](#)]
14. Tolstykh, N.; Vymazalova, A.; Tuhy, M.; Shapovalova, M. Conditions of formation of Au–Se–Te mineralization in the Gaching ore occurrence (Maletoyvayam ore field), Kamchatka, Russia. *Mineral. Mag.* **2018**, *82*, 649–674. [[CrossRef](#)]
15. Tsukanov, N.V. Tectono-stratigraphic terranes of Kamchatka active margins: Structure, composition and geodynamics. In *Materials of the Annual Conference “Volcanism and Related Processes”*; Petropavlovsk-Kamchatsky: Kamchatka Krai, Russia, 2015; pp. 97–103. (In Russian)
16. Golyakov, V.I. *Geological Map of the USSR Scale 1: 200,000*; Pogozhev, A.G., Ed.; Series Koryak; Sheets P-5 8-XXXIII, O-58-III; VSEGEI Cartographic Factory: St. Petersburg, Russia, 1980. (In Russian)
17. Melkomukov, B.H.; Razumny, A.V.; Litvinov, A.P.; Lopatin, W.B. New highly promising gold objects of Koryakiya. *Min. Bull. Kamchatka* **2010**, *14*, 70–74. (In Russian)
18. Palyanova, G.A.; Tolstykh, N.D.; Zinina, V.Y.; Kokh, K.A.; Seryotkin, Y.V.; Bortnikov, N.S. Synthetic chalcogenides of gold in the Au-Te-Se-S system and their natural analogs. *Dokl. Earth Sci.* **2019**, *487*, 929–934.
19. Tolstykh, N.D.; Tuhý, M.; Vymazalová, A.; Plášil, J.; Laufek, F.; Kasatkin, A.V.; Nestola, F. Maletoyvayamite, IMA 2019-021. CNMNC Newsletter No. 50. *Mineral. Mag.* **2019**, *31*. [[CrossRef](#)]
20. Kovalenker, V.A.; Nekrasov, I.Y.; Sandomirskaya, S.M.; Nekrasova, A.N.; Malov, V.S.; Danchenko, V.Y.; Dmitrieva, M.T. Sulfide-selenide-telluride mineralization of epithermal ores in the Kuril-Kamchatka volcanic belt. *Mineral. J.* **1989**, *11*, 3–18. (In Russian)
21. Basso, R.; Cabella, R.; Lucchetti, G.; Marescotti, P.; Martinelli, A. Structural studies on synthetic and natural Fe–Sb–oxides of MO₂ type. *N. Jb. Mineral. Mh.* **2003**, 407–420. [[CrossRef](#)]
22. Kalinin, Y.A.; Palyanova, G.A.; Naumov, E.A.; Kovalev, K.R.; Pirajno, F. Supergene remobilization of Au in Au-bearing regolith related to orogenic deposits: A case study from Kazakhstan. *Ore Geol. Rev.* **2019**, *109*, 358–369. [[CrossRef](#)]
23. Cabri, L.J. Phase relations in the Au–Ag–Te system and their mineralogical significance. *Econ. Geol.* **1965**, *60*, 1569–1605. [[CrossRef](#)]
24. Makovicky, E.; Chovan, M.; Bakos, F. The stibian mustard gold from the Kriván Au deposit, Tatry Mts., Slovak Republic. *N. Jb. Mineral. Abh.* **2007**, *184*, 207–215.
25. Gamyarin, G.N.; Nekrasov, I.; Zhdanov, J.J.; Leskova, I.V. Auroantimonate—A new natural compound of gold. *Dokl. Akad. Nauk SSSR Mineral.* **1988**, *301*, 947–950. (In Russian)
26. Tian, S.; Li, X. A preliminary study of some new minerals in Dongping gold deposit, Hebei province. *Gold Geol.* **1995**, *1*, 61–67.
27. Johan, Z.; Šrein, V. Un nouvel oxide naturel de Au et Sb. *Sci. Terre Planetes* **1998**, *326*, 533–538.
28. Zacharias, J.; Mate, J.N. Gold to aurostibite transformation and formation of Au–Ag–Sb phases: The Krásná Hora deposit, Czech Republic. *Mineral. Mag.* **2017**, *81*, 987–999. [[CrossRef](#)]
29. Zhao, J.; Brugger, J.; Pascal, V.; Gundler, P.; Xia, F.; Chen, G.; Pring, A. Mechanism and kinetics of a mineral transformation under hydrothermal conditions: Calaverite to metallic gold. *Am. Mineral.* **2009**, *94*, 1541–1555. [[CrossRef](#)]
30. Zhao, J.; Xia, F.; Pring, A.; Brugger, J.; Grundler, P.V.; Chen, G. A novel pretreatment of calaverite by hydrothermal mineral replacement reactions. *Miner. Eng.* **2010**, *23*, 451–453. [[CrossRef](#)]
31. Xu, W.; Zhao, J.; Brugger, J.; Chen, G.; Pring, A. Mechanism of mineral transformations in krennerite, Au₃AgTe₈, under hydrothermal conditions. *Am. Mineral.* **2013**, *98*, 2086–2095. [[CrossRef](#)]
32. Xia, F.; Brugger, J.; Chen, G.; Ngathai, Y.; O’Neill, B.; Putnis, A.; Pring, A. Mechanism and kinetics of pseudomorphic mineral replacement reactions: A case study of the replacement of pentlandite by violarite. *Geochim. Cosmochim. Acta* **2009**, *73*, 1945–1969. [[CrossRef](#)]
33. Zhao, J.; Pring, A. Mineral Transformations in Gold–(Silver) Tellurides in the Presence of Fluids: Nature and Experiment. *Minerals* **2019**, *9*, 167. [[CrossRef](#)]
34. Cooke, D.R.; McPhail, D.C. Epithermal Au–Ag–Te mineralization, Acupan, Baguio District, Philippines; numerical simulations of mineral deposition. *Econ. Geol.* **2001**, *96*, 109–131.

35. Kongolo, K.; Mwema, M.D. The extractive metallurgy of gold. *Hyperfine Interact.* **1998**, *111*, 281–289. [[CrossRef](#)]
36. Grosse, A.C.; Dicoski, G.W.; Shaw, M.J.; Haddad, P.R. Leaching and recovery of gold using ammoniacal thiosulfate leach liquors (a review). *Hydrometallurgy* **2003**, *69*, 1–21. [[CrossRef](#)]



© 2019 by the authors. Licensee MDPI, Basel, Switzerland. This article is an open access article distributed under the terms and conditions of the Creative Commons Attribution (CC BY) license (<http://creativecommons.org/licenses/by/4.0/>).